"MULTIPLE SLIP EFFECTS ON NANOFLUID DISSIPATIVE FLOW IN A CONVERGING/ DIVERGING CHANNEL: A NUMERICAL STUDY"

O. Anwar Bég

Professor and Director: Multi-physical Engineering Sciences Group (MPESG), Mechanical Engineering Department, Salford University, Manchester, M54WT, UK, Email: gortoab@gmail.com

Tasveer Bég

Bio-Engineering Mechanics and Geodynamics, Dickenson Road, Manchester, M13, **England, UK,** Email: *tasveerabeg@gmail.com*

W.A. Khan

Department of Mechanical Engineering, College of Engineering, Prince Mohammad Bin Fahd University, Saudia Arabia, Email: wkhan1956@gmail.com

M.J. Uddin*

*Prof. and Head, Department of Mathematics, American International University, Bangladesh, Kuril, Dhaka, 1229, Bangladesh **jashim_74@yahoo.com***

ABSTRACT

A mathematical model is developed for viscous slip flow and heat transfer in water/Ethylene glycol-based nanofluids containing metallic oxide nanoparticles, through a converging/diverging channel geometry. Our approach is based on the single-phase Tiwari–Das nanofluid model considering nanoparticles and base fluid masses as a substitute volume concentration of nanoparticles. The governing (dimensional partial differential) equations are transformed to a set of dimensionless ordinary differential equations with the help of similarity transformation, before being solved numerically using Maple17. Extensive validation of the velocity gradient and temperature solutions is achieved with the second order implicit finite difference Keller Box method (KBM). Further validation is included for the special case of no-slip nanofluid flow in the absence of viscous heating. The effects of the emerging parameters namely velocity slip, thermal jump, channel apex angle, Eckert number, Prandtl number, Reynolds number and nano-particle volume fraction on velocity, temperature, skin friction and heat transfer rate are investigated in detail. Two different nanofluids are studied, namely water-Titanium oxide- and Ethylene glycol-Titanium oxide. Both convergent and divergent channels are addressed, and significantly different thermofluid characteristics are computed due to slip and viscous heating effects. The novelty of the current work is that it extends previous studies to include multiple slip effects and viscous heating (Eckert number effects) which are shown to exert a significant influence on heat and momentum transfer characteristics. The study is relevant to certain pharmaco-dynamics devices (drug delivery), next generation 3-D nanotechnological printers and also nano-cooling systems in energy engineering where laminar flows in diverging/converging channels arise.

Keywords: *Convergent/divergent channel; nanofluids; viscous heating; momentum/thermal slip, nano-engineering devices.*

1. INTRODUCTION

Heat transfer and viscous flows in non-uniform channels (diverging/converging) arise in many branches of applied physics, chemical and biomedical engineering including nozzle designs and protein exchange membrane fuel cells [1-4]. The classical theory of these so-called *Jeffery-Hamel* flows is lucidly documented in Schlichting [5] for Newtonian viscous fluids. Many extensions to the Newtonian case have been reported for a diverse array of complex fluids and with modified boundary conditions and body forces. Balmer and Kauzlaich [6] developed similarity solutions for steady non-Newtonian power law fluid flow in a converging or diverging two-dimensional channel with permeable walls, identifying a singularity caused by the fluid elasticity for the diverging geometry case at Deborah number of unity. Hooper *et al.* [7] studied analytically Jeffery–Hamel flow of a two-fluid system with variable viscosity observing that the velocity distribution becomes discontinuous with an increase in volume flux-based Reynolds number. Hariharan *et al.* [8] used a Fourier series method to investigate peristaltic non-Newtonian flows of power law and Bingham fluids in a diverging tube with various wall wave forms (sinusoidal, multi-sinusoidal, triangular, trapezoidal and square), observing that divergence angle exerts a strong influence on occurrence of reflux near the tube wall even for zero fluxes and the thickness and evolution of the reflux region is markedly affected by the type of wave form. Wu *et al.* [9] conducted a theoretical and experimental study of effective planar micromixer flow featuring a meandering microchannel with converging–diverging cross section, noting that fluid mixing in the microchannel is aided via Dean vortices and in particular the separation vortices generated by the converging–diverging cross section at large flow rate. Lamont *et al.* [10] measured heat transfer coefficient distributions in narrow diverging channels in gas turbine cooling systems. Stalio and Piller [11] used direct numerical simulation to computationally model unsteady forced convection in sinusoidal, symmetric wavy converging/diverging channels.

The above studies did not however consider *nanofluids*. Choi [12] first demonstrated that nanofluids possess enhanced thermophysical properties as compared to conventional heat transfer fluids (lower thermophysical properties). Nanofluids designate a solid-liquid mixture consisting of a fluid suspension having ultra-fine nanoparticles. The size of these suspended particles is typically of the order of few nano meters. The commonly used nanoparticles are Al_2O_3, CuO, TiO_2, ZnO and SiO_2. The significant features of nanofluids include higher thermal conductivity and viscosity as compared to the base fluid and stable nature of the suspension. The volume fraction of nanoparticles is normally engineered to be 3% to 5% so that the

nanofluid exhibit mechanical behavior similar to the base fluid. In recent years nanofluids have filtered into an incredibly diverse number of industries including petroleum [13], medical [14], chemical polymer coating [15], wound treatment [16], nano-materials processing [17, 18], microbial fuel cell enhancement [19], drug delivery (pharmaco-dynamics) [20] and even protein detection technologies [21]. Comprehensive reviews of heat transfer characteristics of nanofluids have been presented in [22-25]. Extensive efforts have been made to develop robust mathematical models for the thermal conductivity enhancement features of nanofluids. Suggested mechanisms for this include *dispersion of nanoparticles, turbulence and micro-convection, and also rotation of the nanoparticles*. A popular model which is relatively simple to implement is that of Tiwari and Das [26] in which nanoparticle contribution is simulated via volume fraction rather than in a separate species conservation equation. His model has been employed to analyse a variety of metal-oxide nanofluids including zinc oxide, copper oxide, titanium oxide, aluminium oxide and others. Recent studies employing the Tiwari-Das formulation include Tripathi and Bég [27] who considered peristaltic propulsion of nanofluids in pharmacological systems. In the context of diverging channel flows, Akbar and Nadeem [28] used the Tiwari-Das approach to simulate peristaltic transport of viscoelastic nanofluids. Recently, various applications of the Tiwari-Das nanofluid model [26] have been analysed by a number of researchers [29-32].

In the present study we use **MAPLE17** numerical quadrature [33] to study the dissipative nanofluid flow and heat transfer in a converging/diverging channel with the Tiwari-Das model. Solutions are obtained for the velocity, temperature, wall shear stress and heat transfer rate (Nusselt number) distributions for a variety of the emerging parameters. Verification of the solutions for the general slip model is attained with the implicit finite difference Keller Box Method (**KBM**). Further validation for the no-slip case is conducted with the no-slip case reported by Moradi *et al.* [35] in the absence of viscous heating. The transformed ordinary differential boundary value problem, which is nonlinear, also provides a good benchmark for further more elaborate numerical simulations with for example computational fluid dynamics (CFD) codes [34] and significantly extends earlier investigations which have been confined to Jeffery-Hamel *non-slip flows without viscous heating effects* [35]. The present work extends the current research by including slip (momentum and thermal) and viscous heating effects for the first time in nanofluid Jeffrey-Hamel flows. It is relevant to cooling enhancement in energy systems and also biomedical devices (nozzle delivery) employing nanofluids where

diverging/converging channels feature in novel nozzle configurations, diffusers, inlet and outlet geometries.

2. MATHEMATICAL NANOFLUID MODEL

The flow model and coordinate system is displayed in **Fig. 1**, in a polar (r, θ) coordinate system. Nanofluid flow from a source/sink is studied at the apex of a converging/diverging channel (i.e. *non-parallel* solid walls intersecting) with intersection angle 2α.
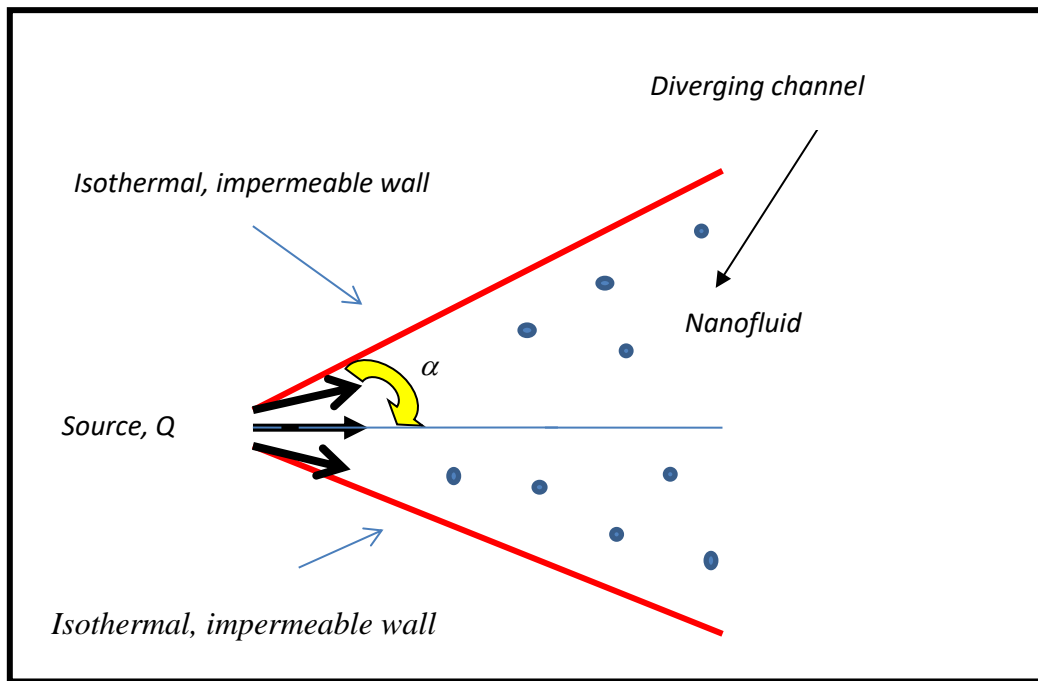
Fig 1: Nanofluid Jeffery-Hammel flow geometry (diverging case)

Forced convection heat transfer takes place. Thermal dispersion and heat generation effects are neglected. With viscous dissipation present, which is important in incompressible flows, by means of Tiwari–Das nanofluid's model (Tiwari and Das [26]), the appropriate balance equations for two-dimensional Jeffery-Hamel nanofluid flow are the mass, momentum and heat conservation which are given below (Dinarvand and Rostami [29]).

$$\nabla \cdot \mathbf{v} = 0 \tag{1}$$

$$\rho \left[\frac{\partial \mathbf{v}}{\partial t} + (\mathbf{v} \cdot \nabla) \mathbf{v} \right] = -\nabla p + \mu \nabla^2 \mathbf{v}, \tag{2}$$

$$\frac{\partial T}{\partial t} + \mathbf{v} \times \nabla \mathrm{T} = \alpha \nabla^2 T \tag{3}$$

Here $\mathbf{v}$ is velocity vector, T is temperature. $\nabla^2 = \frac{\partial^2}{\partial r^2} + \frac{1}{r}\frac{\partial}{\partial r} + \frac{1}{r^2}\frac{\partial}{\partial \theta^2}$. The conservation equations in polar coordinates in the absence of body forces and under aforementioned assumptions become:

Mass conservation:
$$\frac{\rho_{nf}}{r}\frac{\partial(ru)}{\partial r} = 0 \tag{4}$$

r-Momentum conservation:
$$u\frac{\partial u}{\partial r} = -\frac{1}{\rho_{nf}}\frac{\partial p}{\partial r} + \frac{\mu_{nf}}{\rho_{nf}}\left(\frac{\partial^2 u}{\partial r^2} + \frac{1}{r}\frac{\partial u}{\partial r} + \frac{1}{r^2}\frac{\partial^2 u}{\partial \theta^2} - \frac{u}{r^2}\right) \tag{5}$$

θ-Momentum conservation:
$$-\frac{1}{\rho_{nf} r}\frac{\partial p}{\partial \theta} + \frac{2\mu_{nf}}{\rho_{nf} r^2}\frac{\partial u}{\partial \theta} = 0 \tag{6}$$

Heat (energy) conservation:
$$u\frac{\partial T}{\partial r} = \alpha_{nf}\left(\frac{\partial^2 T}{\partial r^2} + \frac{1}{r}\frac{\partial T}{\partial r} + \frac{1}{r^2}\frac{\partial^2 T}{\partial \theta^2}\right) + \frac{\mu_{nf}}{(\rho C_p)_{nf}}\left(4\left[\frac{\partial u}{\partial r}\right]^2 + \frac{1}{r^2}\left[\frac{\partial u}{\partial \theta}\right]^2\right) = 0 \tag{7}$$

The appropriate boundary conditions are specified as follows:

Symmetry (channel centre line): $\quad \frac{\partial u}{\partial \theta} = 0; \frac{\partial T}{\partial \theta} = 0, u = U \tag{8a}$

Wall (-slip): $\quad \mathrm{u} = -\mathrm{N_1}\nu_{nf}\frac{\partial \mathrm{u}}{\partial \theta}; \mathrm{T} = \mathrm{T_w} - \mathrm{N_1}\frac{\partial \mathrm{T}}{\partial \theta} \tag{8b}$

Here U is an arbitrary velocity, u is radial velocity, T is temperature, p is pressure. The effective density ρ_{nf}, the effective dynamic viscosity μ_{nf}, the effective heat capacity $(\rho C_p)_{nf}$, effective thermal conductivity k_{nf} and thermal diffusivity α_{nf} of the nanofluid are defined following Tiwari and Das [26] as follows:

$$\rho_{nf} = (1-\varphi)\rho_f + \varphi\rho_s, \quad \mu_{nf} = \frac{\mu_f}{(1-\varphi)^{2.5}}, \quad (\rho C_p)_{nf} = (1-\varphi)(\rho C_p)_f + \varphi(\rho C_p)_s$$

(9a)

$$\frac{k_{nf}}{k_f} = \frac{k_s + 2k_f - 2\varphi(k_f - k_s)}{k_s + 2k_f + 2\varphi(k_f - k_s)},$$

$$\alpha_{nf} = \frac{k_{nf}}{(\rho C_p)_{nf}}$$

(9b)

Here ϕ is the solid volume fraction of the nanoparticles, ρ_f is the base fluid density, ρ_s is the nanoparticle (solid) density and μ_f is the base fluid dynamic viscosity. The nonlinear primitive boundary value problem defined by Eqns. (4)-(7) under boundary conditions (5a, b) generally required a numerical solution via explicit finite differences or a finite element method. It can however be significantly simplified by observing from the continuity equation that the radial velocity, u, must be of the form:

$$f = ur$$

(10)

We further introduce the following similarity variables:

$$F = \frac{f}{rU}; \quad \eta = \frac{\theta}{\alpha}; \quad \Theta = \frac{T}{T_w}$$

(11)

where F is a dimensionless radial velocity function, η is dimensionless angular coordinate and Θ is non-dimensional temperature. Elimination of the pressure, p, between Eqns. (5) and (6) leads to:

Momentum:

$$\frac{d^3 F}{d\eta^3} + 2\alpha\,\text{Re}[(1-\varphi)^{2.5}(1-\varphi+\varphi\frac{\rho_s}{\rho_f}]F\frac{dF}{d\eta} + 4\alpha^2\frac{dF}{d\eta} = 0$$

(12)

Energy:

$$\frac{1}{\left(1-\varphi+\varphi\dfrac{(\rho C_p)_s}{(\rho C_p)_f}\right)}\left[\frac{k_{nf}}{k_f}\frac{d^2\Theta}{d\eta^2} + \frac{\Pr Ec}{(1-\varphi)^{2.5}}\left[4\alpha^2 F^2 + \left(\frac{dF}{d\eta}\right)^2\right]\right] = 0$$

(13)

The transformed boundary conditions take the form:

$$At\ \eta = 0: F(0) = 1; \quad \frac{dF(0)}{d\eta} = 0; \frac{d\Theta(0)}{d\eta} = 0$$

(14)

As $\eta \rightarrow 1 : F(1) = -\dfrac{1}{(1-\phi)^{2.5}(1-\phi+\phi\dfrac{\rho_s}{\rho_f})}\, a\, F'(1); \;\; \Theta(1) = 1 - b\, \Theta'(1)$ \hfill (15)

In Eqns. (12) and (13), the Reynolds number (Re), Eckert number (Ec) and Prandtl number (Pr) and velocity slip (a), thermal slip (b) are defined as:

$$Re = \frac{U_{max}r\rho_f\alpha}{\mu_f}, Ec = \frac{U^2}{(c_p)_f T_w}, Pr = \frac{\mu_f(C_p)_f}{k_f}, a = \frac{N_1\nu_f}{\alpha}, b = \frac{D_1}{\alpha}$$ \hfill (16)

For a *diverging* channel, in the Reynolds number $\alpha>0$, $U_{max}>0$; for the *converging* channel case, $\alpha<0$, $U_{max}<0$. In engineering simulations we are interested not only in the velocity and temperature functions, but also certain gradient functions of these variables. The non-dimensional skin friction coefficient, C_f, may be defined in terms of transformed variables, thus:

$$C_f = \frac{\tau_w}{\rho_{nf}U_{max}^2} = \frac{1}{Re(1-\phi)^{2.5}}\frac{dF(1)}{d\eta}$$ \hfill (17)

Here the shear stress at the walls, τ_w, is:

$$\tau_w = \frac{\mu_{nf}}{r}\frac{du}{d\theta}$$ \hfill (18)

The dimensionless Nusselt number (wall heat transfer rate) is given by:

$$Nu = \frac{rq_w\,|_{\theta=\alpha}}{k_f T_w} = -\frac{rk_{nf}\dfrac{dT}{dr}\,|_{\theta=\alpha}}{k_f T_w}$$ \hfill (19)

In terms of the transformed variables we have:

$$Nu = -\frac{1}{\alpha}\frac{k_{nf}}{k_f}\frac{d\Theta(1)}{d\eta}$$ \hfill (20)

The fifth order nonlinear boundary value problem described in Eqns. (12)-(13) under boundary conditions (14), (15) is unlikely to yield analytical solutions. We therefore develop numerical solutions using **MAPLE17**. The methodology is described in detail in [36-38]. Several important special cases of the present flow model may be retrieved. The flow model describes Newtonian Jeffery-Hamel flow as $\varphi \rightarrow 0$ (nanoscale effects vanish). When $Ec =0$ viscous

heating is negated. When both nanoscale and viscous heating effects are omitted the model reduces to that studied in [35]. In the general model, a homogenous distribution of nanoparticles is assumed in the nanofluid i.e. a *dilute* suspension. The nanofluid consists of *two-component* mixtures (nano-solid-particles and the base fluid are in thermal equilibrium) and no slip occurs between them. Slip arises *only* at the channel walls.

3. MAPLE SOLUTIONS

The boundary value problem (BVP) is solved using **MAPLE 17** numerical integration quadrature based on Runge-Kutta Fehlberg shooting algorithms. This is a highly efficient methodology for BVPs with infinity boundary conditions. A Runge–Kutta–Fehlberg fourth-fifth order numerical algorithm (**RKF45**) is employed, which is readily available in the symbolic computer software **MAPLE17**. This method has been employed extensively in fluid mechanics simulations, including nanofluid dynamics e.g. radiative slip flow of magnetic nanofluids [37], magnetic nanofluid flow from a stretching surface [38], power-law nanofluid flow in porous media [39]. Other applications include Marangoni (surface-tension) driven nanofluid transport in biopolymers [40] and non-Newtonian petrochemical mass transfer in porous media [41]. The RK45 algorithm is based on a *collocation method* in which a finite-dimensional space of candidate solutions is selected (usually, polynomials up to a certain degree) and a number of points in the domain (called *collocation points*), and a solution selected which satisfies the given equation at the collocation points. The details of **RFK45** methods can be found in the ref. [37, 38]. MAPLE is an excellent symbolic software with many libraries of built in ready-to-use numerical solvers for ordinary and partial differential problems. In MAPLE the RK45 quadrature is used to yield temperature and stream function. The appropriate velocity is then computed in a sub-iteration loop. The robustness and stability of this numerical method is therefore well established- it is highly adaptive since it adjusts the quantity and location of grid points during iteration and thereby constrains the local error within acceptable specified bounds. Many different wall boundary conditions are easily accommodated. The stepping formulae although designed for nonlinear problems, are even more efficient for any order of linear differential equation and are summarized below [**37**]:

$$k_0 = f\left(x_i, y_i\right), \tag{21}$$

$$k_1 = f\left(x_i + \frac{1}{4}h, y_i + \frac{1}{4}hk_0\right), \tag{22}$$

$$k_2 = f\left(x_i + \frac{3}{8}h, y_i + \left(\frac{3}{32}k_0 + \frac{9}{32}k_1\right)h\right), \tag{23}$$

$$k_3 = f\left(x_i + \frac{12}{13}h, y_i + \left(\frac{1932}{2197}k_0 - \frac{7200}{2197}k_1 + \frac{7296}{2197}k_2\right)h\right), \tag{24}$$

$$k_4 = f\left(x_i + h, y_i + \left(\frac{439}{216}k_0 - 8k_1 + \frac{3860}{513}k_2 - \frac{845}{4104}k_3\right)h\right), \tag{25}$$

$$k_5 = f\left(x_i + \frac{1}{2}h, y_i + \left(-\frac{8}{27}k_0 + 2k_1 - \frac{3544}{2565}k_2 + \frac{1859}{4101}k_3 - \frac{11}{40}k_4\right)h\right), \tag{26}$$

$$y_{i+1} = y_i + \left(\frac{25}{216}k_0 + \frac{1408}{2565}k_2 + \frac{2197}{4101}k_3 - \frac{1}{5}k_4\right)h, \tag{27}$$

$$z_{i+1} = z_i + \left(\frac{16}{135}k_0 + \frac{6656}{12825}k_2 + \frac{28561}{56430}k_3 - \frac{9}{50}k_4 + \frac{2}{55}k_5\right)h. \tag{28}$$

Here y denotes fourth order Runge-Kutta phase and z is the fifth order Runge-Kutta phase. An estimate of the error is achieved by subtracting the two values obtained. If the error exceeds a specified threshold, the results can be re-calculated using a smaller step size. The approach to estimating the new step size is shown below:

$$h_{new} = h_{old}\left(\frac{\varepsilon h_{old}}{2|z_{i+1} - y_{i+1}|}\right)^{1/4}. \tag{29}$$

The **MAPLE17** code has been extensively validated for many nonlinear problems [37-41] and confidence in the current computations is very high. In order to analyse the sensitivity of the physical model to different thermophysical parameters, extensive computations have been conducted and are documented in **Figs. 2-11**. In each case the following nanofluid properties must be determined in eqns. (9), (10) i.e. $\dfrac{\rho_s}{\rho_f}$ (density ratio in eqn (9)) and $\dfrac{(\rho C_p)_s}{(\rho C_p)_f}$ (i.e. specific heat capacity ratio) and $\dfrac{k_{nf}}{k_f}$ (i.e. thermal conductivity ratio) in eqn. (10). We examine a number of nanofluids e. g. water-Titanium oxide- and Ethylene glycol - Titanium oxide, as documented in [26]. Further graphs can be generated for Aluminium oxide and copper oxide, using

properties [27]. Velocity gradient, temperature, skin friction and Nusselt number are all computed.

4. VALIDATION OF GENERAL MODEL WITH KELLER BOX METHOD (KBM)

In order to justify our results, the Keller-Box implicit difference method (**KBM**) is also used to solve the same equations. This second order accurate method is ideal for *parabolic* problems e.g. boundary layer flows, although it can be used for fully developed channel flows also. Recently the **KBM** algorithm has successfully resolved a number of nonlinear magnetohydrodynamics and nanofluid dynamics problems including micropolar nanofluid enrobing flows [42], Hall MHD generator transport [43], viscoelastic flows in porous media [44] and biological micro-organism propulsion [45]. The detail of the KBM is elaborated by Keller [46]. The numerical algorithm is performed in **MATLAB** on an Octane SGI workstation and computes in seconds. The method demonstrates excellent stability, convergence and consistency, as elaborated by Keller [47]. In KBM, there are 4 key steps:

(I)Reduction of Eqns. (12) - (13) into a system of first order ordinary differential equations. Thus, the coupled differential equations of third order in F (η) and second order in Θ (η) are reduced to a system of five simultaneous equations of first order for five unknowns. Boundary conditions (14 and (15) are also transformed.

(II)In the second step derivatives are approximated in the new system of first order equations with central difference approximations by considering a net rectangle in the $x\eta - plane$ and the net points are defined as $\eta_0 = 0, \eta_j = \eta_{j-1} + h_j$ $n = 1, 2, 3...J; j = 1, 2, 3...J$ and $\eta_j = \eta_\infty$. Here h_j is the $\Delta\eta - spacing$ and n, j are just the sequences of numbers that indicate the coordinate location. The centering midpoint $\left(\eta_{j-\frac{1}{2}}\right)$ of the segment is obtained by using the following finite difference approximations.

$$(\ )^n_{j-\frac{1}{2}} = \frac{1}{2}\left[(\ )^n_j + (\ )^n_{j-1}\right]; \quad \left(\frac{\partial(\ )}{\partial\eta}\right)^{n-\frac{1}{2}}_{j-\frac{1}{2}} = \frac{1}{h_j}\left[(\ )^{n-\frac{1}{2}}_j + (\ )^{n-\frac{1}{2}}_{j-1}\right]; \qquad (30)$$

(III) In the third step the emerging nonlinear algebraic equations are linearized with Newton's method by using iterates of the form $( )^{i+1}_j = ( )^i_j + \delta( )^i_j$ and then cast into matrix vector form.

(IV) Finally, in the fourth step, the linearized algebraic equations are solved using a block tri-diagonal elimination scheme implemented in MATLAB software with the suitable initial solution. This method is unconditionally stable has a second order accuracy and is relatively easy to program, thus making it highly attractive for engineering analysis. For this iterative scheme to solve the system of equations, a convergence criterion is required. This is specified

as follows: when the difference between two successive approximations is sufficiently small ($\leq 10^{-5}$) the solutions are taken to have converged to the requisite accuracy.

Comparison computations (which relate to the appropriate **MAPLE 17** green dotted lines only) are denoted by the *blue triangles* in **Figs 2a, 3a, 4a, 5a** and **6a.** In each graph in other words we have verified one **MAPLE17** solution and excellent agreement is achieved. Confidence in **MAPLE17** shooting solutions is therefore justifiably high.

5. VALIDATION WITH NO-SLIP CASE AND ABSENCE OF VISCOUS HEATING

Due to unavailability of experimental data, it is not possible to compare with the experimental data. However, we have included a comparison table with the published data of a simpler previous study [35]. Tables 1 and 2 are comparisons of the MAPLE 17 code for the special reduced no-slip (N_1 =0) case and for zero volume fraction ($\phi = 0$) with [35]. At all Reynolds numbers and vertex angles of the diverging/converging channel, excellent correlation is achieved for the stream function $f(\eta)$ and skin friction f''(0) with MAPLE RK45 and the solutions of Moradi *et al*. [35]. Confidence in the MAPLE RK45 code is therefore justifiably very high.

Table 1: Numerical values of the function $f(\eta)$ for Newtonian fluid ($\phi = 0$)

η	Moradi et al. [35] numerical results			Present numerical results		
	$Re = 110$ $\alpha = 3^o$	$Re = 80$ $\alpha = -5^o$	$Re = 50$ $\alpha = 5^o$	$Re = 110$ $\alpha = 3^o$	$Re = 80$ $\alpha = -5^o$	$Re = 50$ $\alpha = 5^o$
0	1	1	1	1	1	1
0.1	0.979236	0.995961	0.982431	0.97923571	0.99596063	0.98243124
0.2	0.919266	0.983276	0.931226	0.91926589	0.98327554	0.93122597
0.3	0.826534	0.96018	0.850611	0.82653362	0.96017991	0.85061063
0.4	0.710221	0.923522	0.746792	0.71022119	0.92352159	0.74679081
0.5	0.580499	0.868459	0.626849	0.58049946	0.86845888	0.62694818
0.6	0.446935	0.788091	0.498234	0.44693507	0.78809092	0.49823446
0.7	0.317408	0.673144	0.366966	0.31740843	0.67314363	0.36696635
0.8	0.197641	0.511991	0.238124	0.19764109	0.51199109	0.23812375
0.9	0.09123	0.291559	0.115152	0.09123042	0.29155874	0.11515193
1	0	0	0	0	0	0

Table 2: Numerical values of skin friction for Newtonian fluid ($\phi = 0$)

$\alpha = 0.1$	Moradi et al. [35]		Present results	
	TiO₂	Cu	TiO₂	Cu
Re = 10	−0.236316	−0.228015	−0.23631589	−0.22801492
Re = 30	−0.0630751	−0.0547215	−0.063075067	−0.05472165
Re = 50	−0.0284339	−0.023245	−0.028433869	−0.02324493
$\alpha = 0.2$				
Re = 10	−0.319488	−0.302882	−0.31948789	−0.30288148
Re = 30	−0.0869483	−0.070249	−0.086948288	−0.07024876
Re = 50	−0.0404258	−0.0241233	−0.040425766	−0.024123292

## 6. MAPLE17 COMPUTATIONAL RESULTS AND DISCUSSION

Figs 2a,b illustrate the evolution of non-dimensional velocity gradient for water-TiO₂ and ethylene glycol- TiO₂ nanofluids, with nanoparticle volume fraction (ϕ) and momentum slip parameter (*a*). The evolution of velocity has already been elaborated in other studies e.g. Moradi *et al.* [35] and is well-known. We therefore elect here to examine velocity gradient response instead. In all figures the viscous heating is strong (*Ec* = 5), the channel is *diverging* ($\alpha = 3°$), flow is *laminar* (*Re* =50) and the *thermal slip* is weak (*b* = 0.5). The range $0 \leq \eta \leq 1$ corresponds to the channel semi-space i.e. from the longitudinal axis to the upper wall. Since reflective symmetry is achieved via the boundary conditions and geometry it is not necessary to plot the lower semi-space.
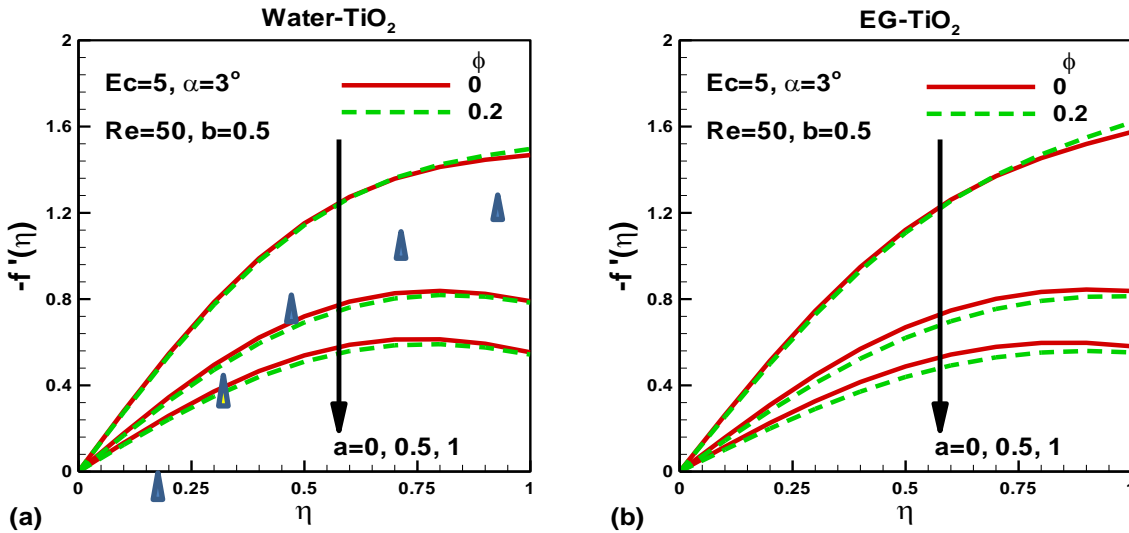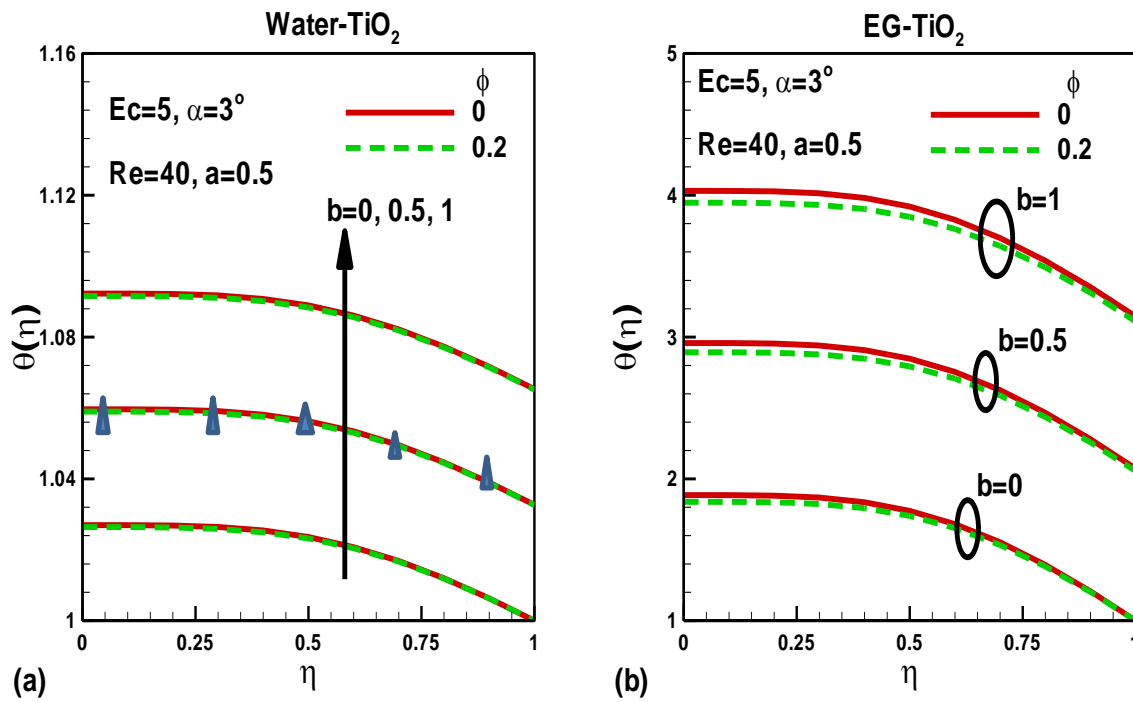

Fig. 2: Effects of volume fraction of nanoparticles and slip parameter on dimensionless velocity gradient for (a) Water-TiO₂ and (b) EG-TiO₂ nanofluids. [Blue triangles represent the appropriate KBM solution validating the green dotted line MAPLE17 case].
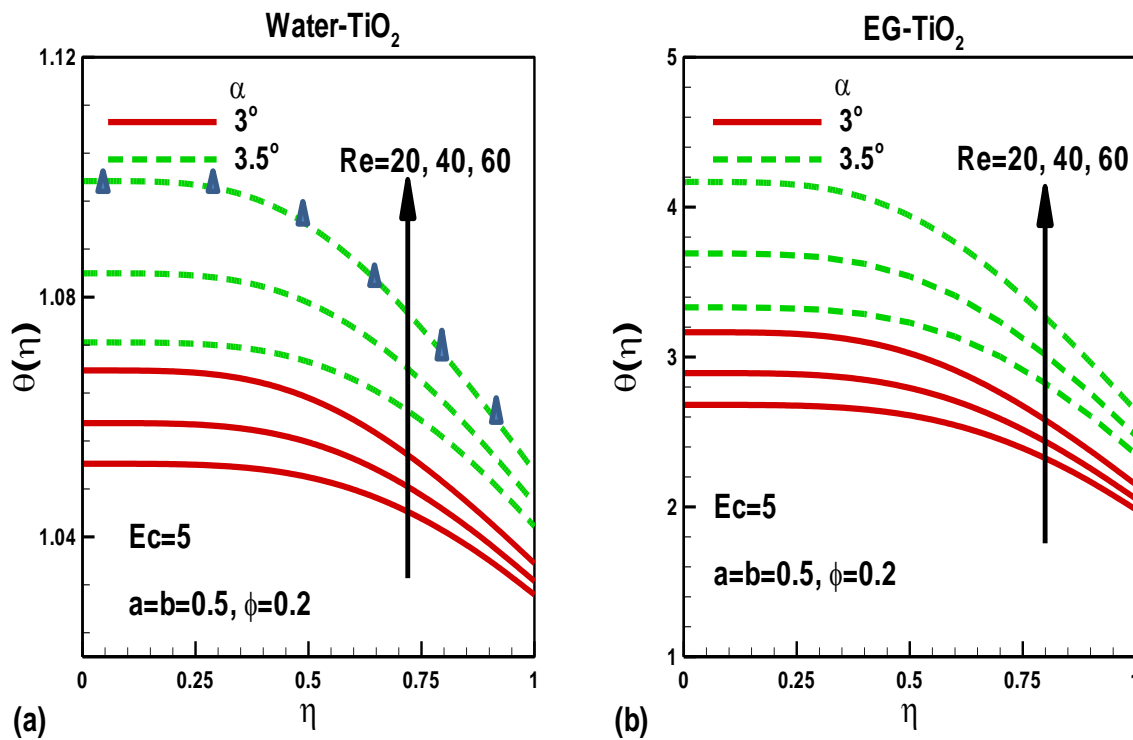
13
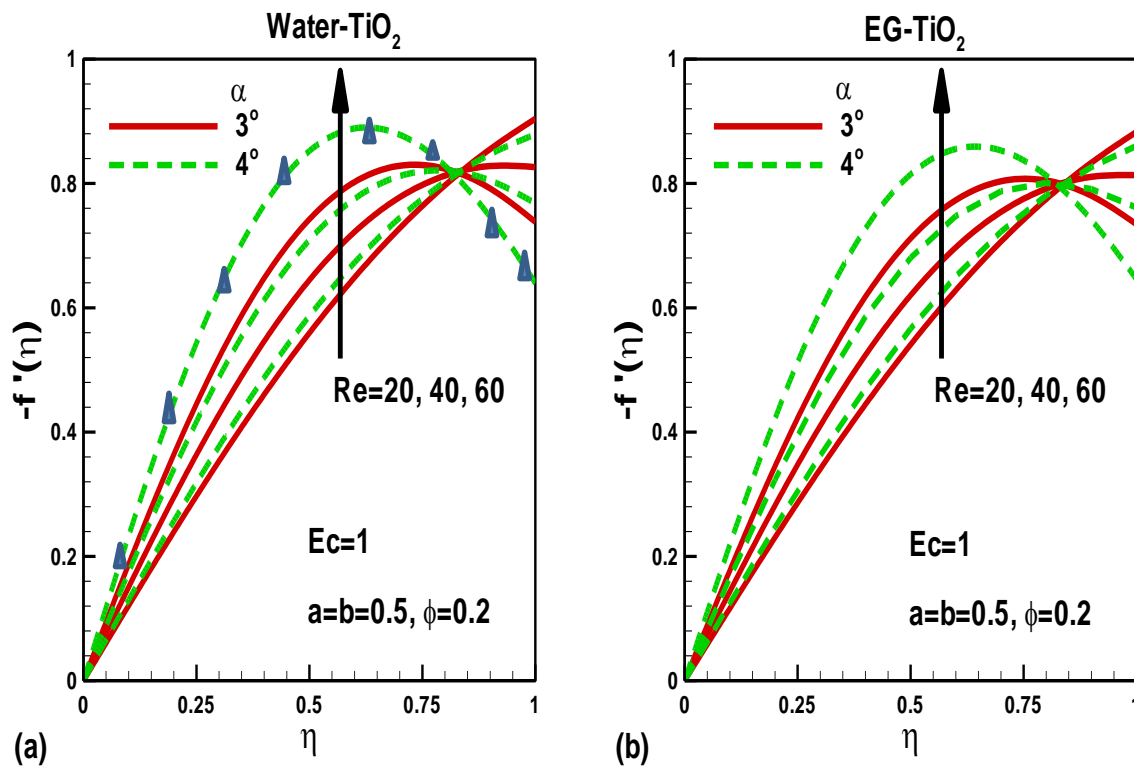
Fig. 3: Effects of *converging* channel angle and Reynolds number on dimensionless velocity gradient for (a) Water-TiO$_2$ and (b) EG-TiO$_2$ nanofluids. [Blue triangles represent the appropriate KBM solution validating the green dotted line MAPLE17 case].
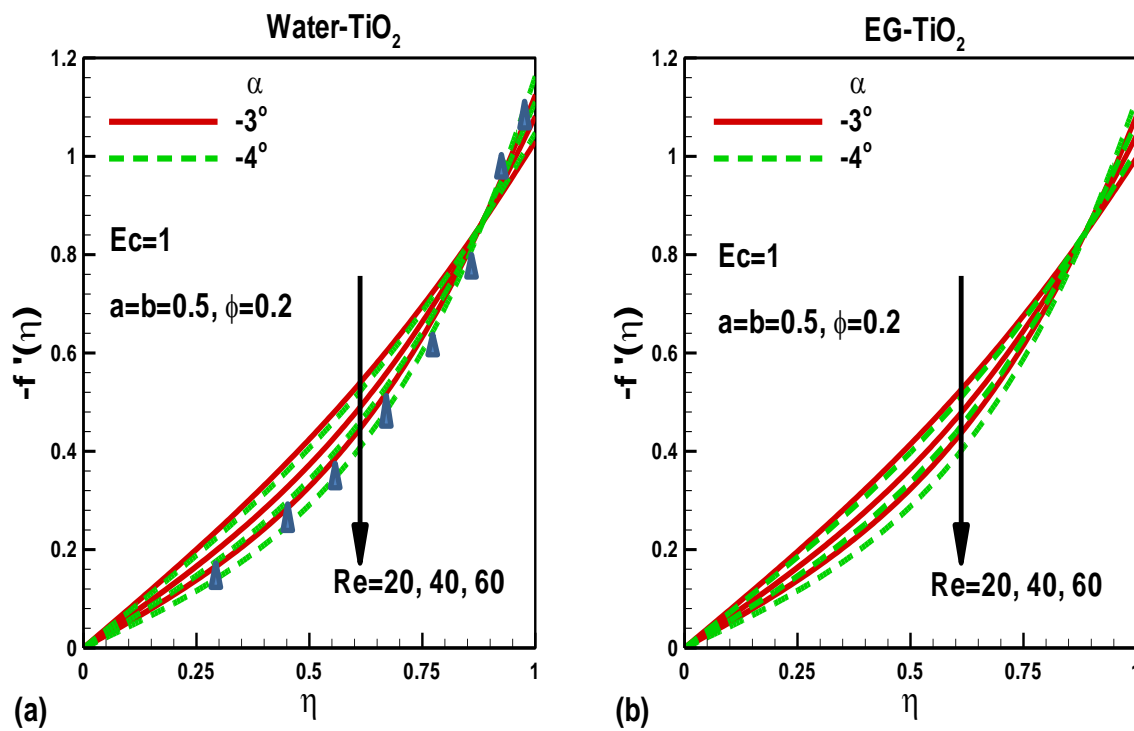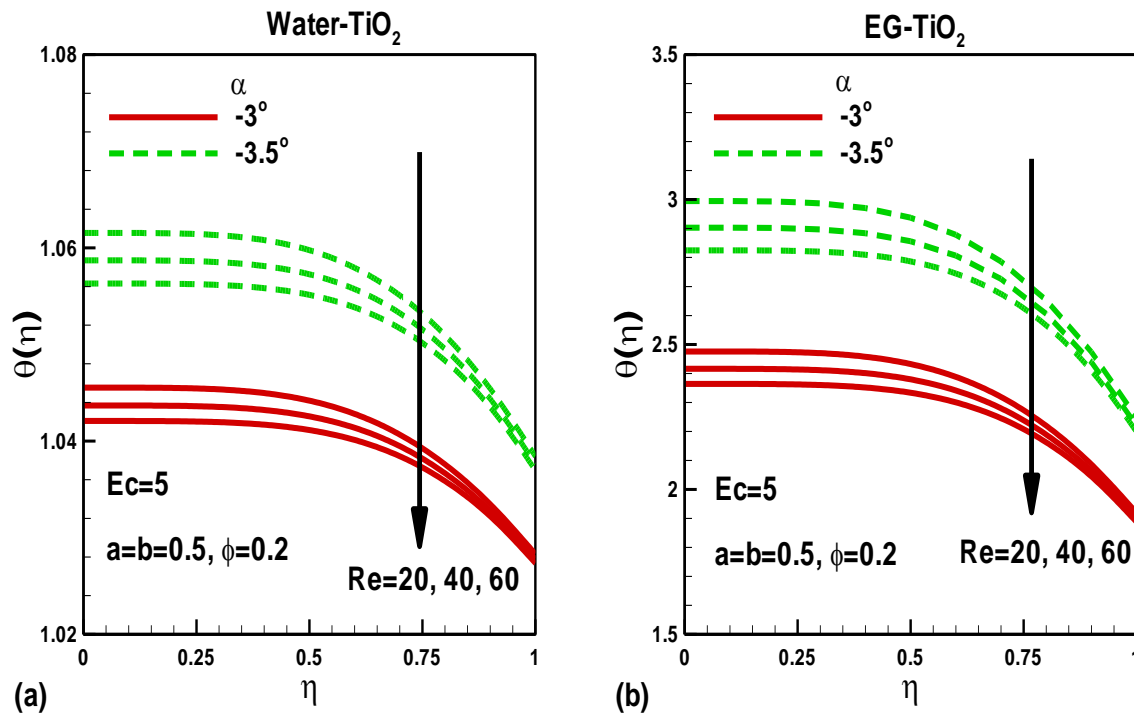

Fig. 4: Effects of *diverging* channel angle and Reynolds number on dimensionless velocity gradient for (a) Water-TiO$_2$ and (b) EG-TiO$_2$ nanofluids. [Blue triangles represent the appropriate KBM solution validating the green dotted line MAPLE17 case].

Fig. 5: Effects of volume fraction of nanoparticles and thermal slip parameter on dimensionless temperature for (a) Water-TiO₂ and (b) EG-TiO₂ nanofluids. [Blue triangles represent the appropriate KBM solution validating the green dotted line MAPLE17 case].


Fig. 6: Effects of converging channel angle and Reynolds number on dimensionless temperature for (a) Water-TiO₂ and (b) EG-TiO₂ nanofluids. [Blue triangles represent the appropriate KBM solution validating the green dotted line MAPLE17 case].
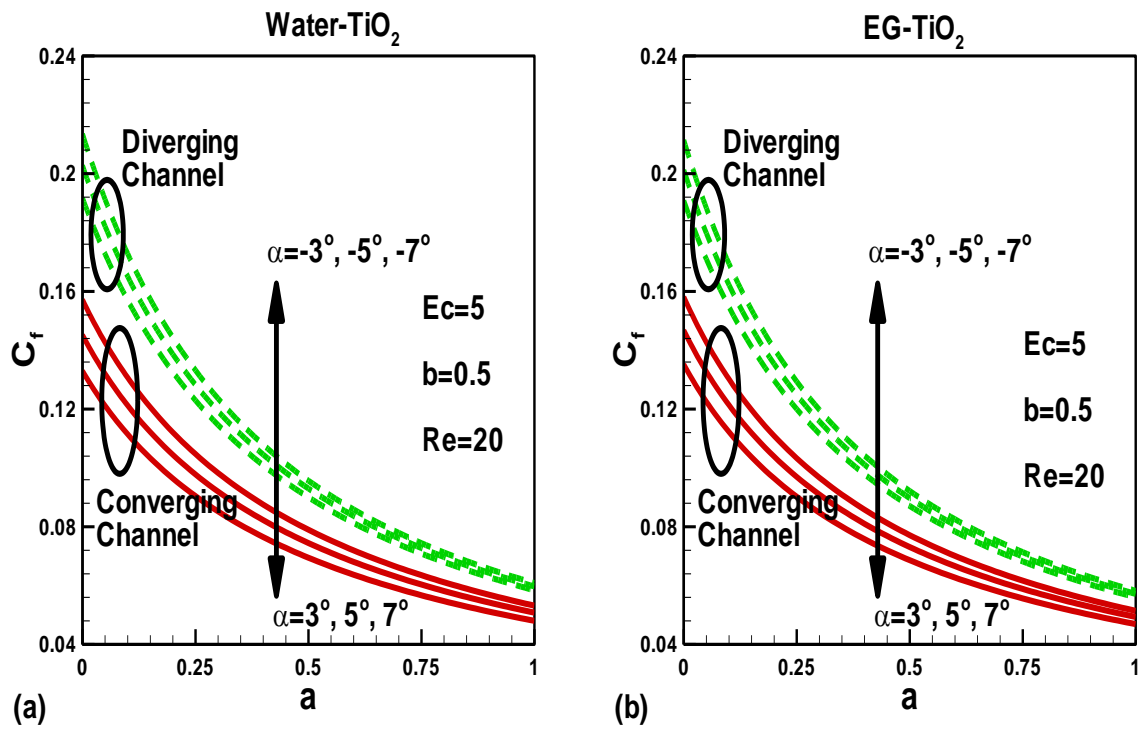
Fig. 7: Effects of diverging channel angle and Reynolds number on dimensionless temperature for (a) Water-TiO$_2$ and (b) EG-TiO$_2$ nanofluids.
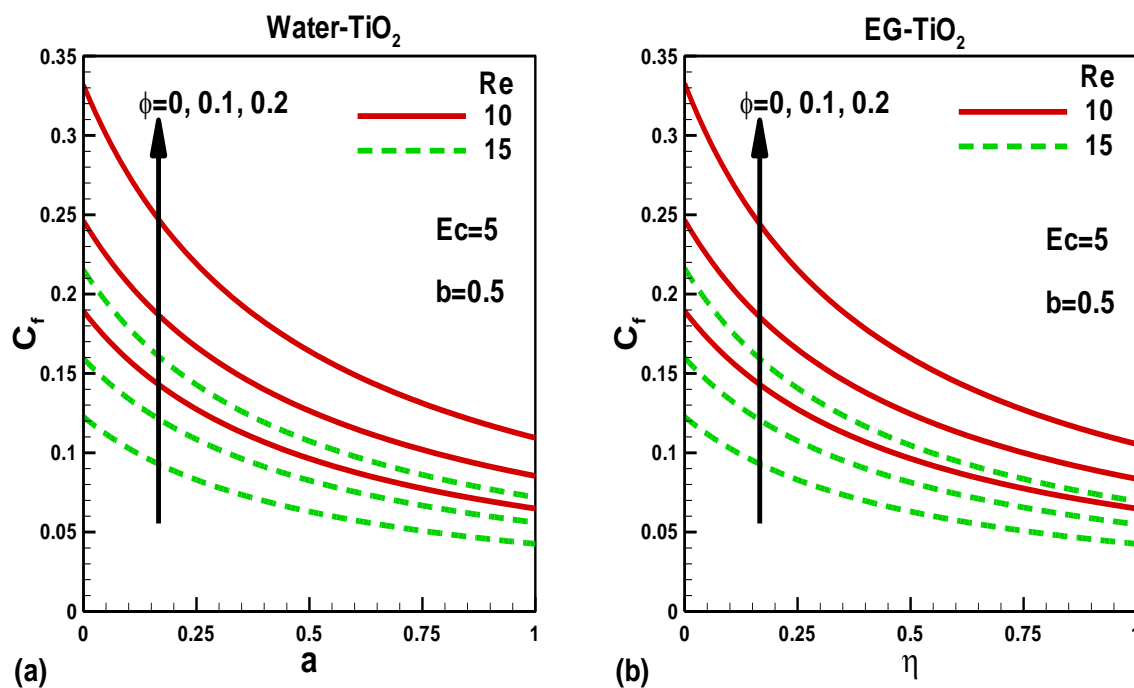
Fig. 8: Skin friction as a function of velocity slip, volume fraction of nanoparticles and Reynolds number for (a) Water-TiO$_2$ and (b) EG-TiO$_2$ nanofluids (converging case).
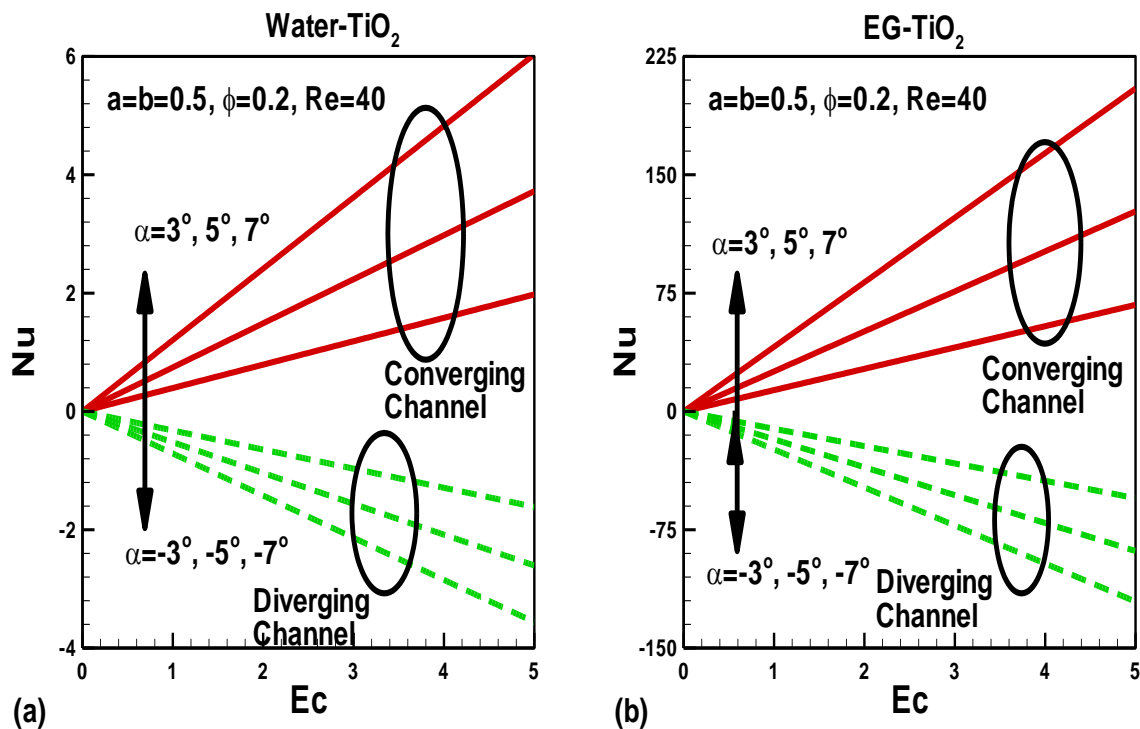
Fig. 9: Skin friction as a function of velocity slip and converging-diverging channel angles for (a) Water-TiO$_2$ and (b) EG-TiO$_2$ nanofluids.
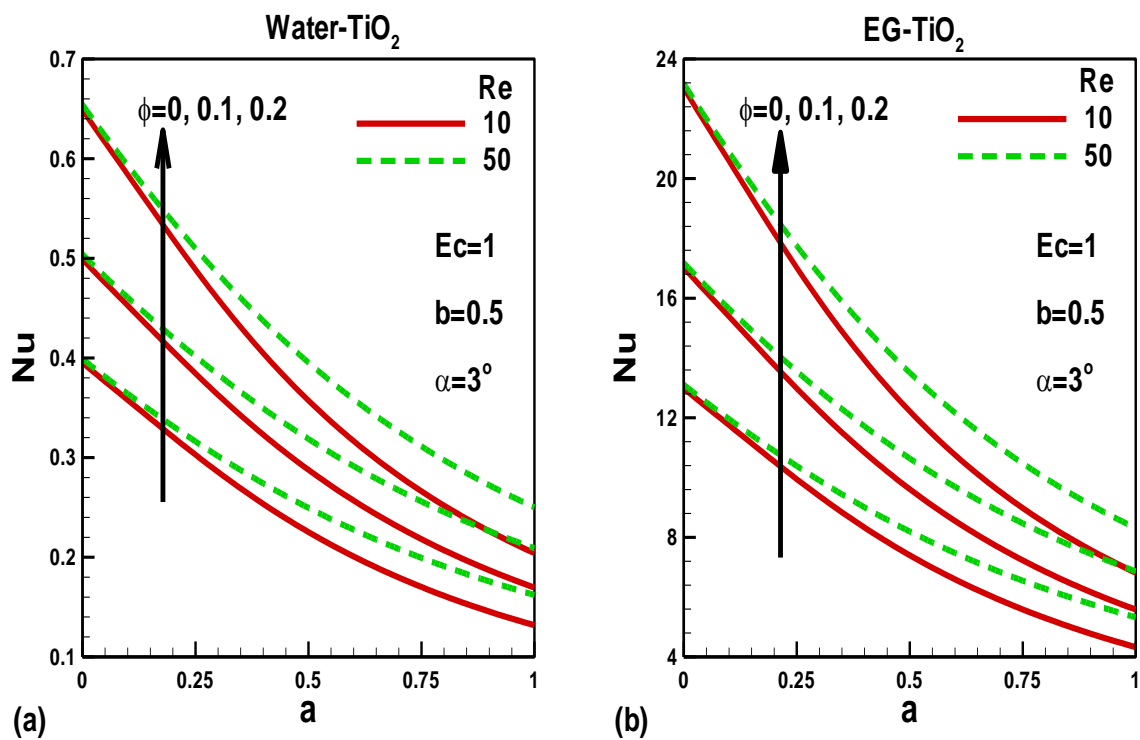
Fig. 10: Nusselt numbers as function of velocity slip, volume fraction of nanoparticles and Reynolds number for (a) Water-TiO$_2$ and (b) EG-TiO$_2$ nanofluids.

Fig. 11: Nusselt numbers as a function of Eckert number and converging-diverging channel angles for (a) Water-TiO₂ and (b) EG-TiO₂ nanofluids.

Radial velocity gradient (which is prescribed zero magnitude at the channel centre line) grows steadily from the centre line ($\eta = 0$) towards the channel wall; however with greater momentum slip, it peaks in close proximity to the wall and not at the wall, whereas in the absence of slip it attains a maximum at the wall. With greater momentum slip for both the both water-TiO₂ and ethylene glycol-TiO₂ nanofluids [46], velocity gradient is depressed indicating that the nanofluid shears slower and decelerates. With increasing nanoparticle volume and momentum slip present ($a = 0.5, 1$) the velocity gradient is reduced for both nanofluids. However in the no-slip case ($a = 0$) this behaviour although present for most of the channel half space, is reversed near the wall where volume fraction increasing is observed to elevate velocity gradient. Generally therefore flow deceleration accompanies greater volume fractions with velocity slip present whereas the converse behaviour is observed in the no-slip scenario.

Figs 3a,b present the radial velocity gradient distributions with varying Reynolds number (*Re*) and channel semi-vertex angle (α). Only converging channel cases are examined ($\alpha > 0$). Generally for the most part of the semi-channel space, increasing Reynolds number serves to accelerate the flow and increases velocity gradient magnitudes. With increasing semi-vertex

angle, acceleration is also caused in this large extent of the channel semi-space. However closer to the wall (boundary), the reverse effect is computed. The nanofluid flow is markedly decelerated, although not to the same degree as the acceleration in the zone far from the wall. The inertial body force associated with larger Reynolds numbers is therefore counter-productive in the near-wall zone whereas it is beneficial in the near centre-line zone. The implication is that enhanced momentum transfer is achieved closer to the symmetry axis of the channel rather than near the boundary, with greater inertial effects. With wider vertex angles of the channel, the velocity is also boosted near the channel centre and around this zone as compared with the boundary (wall) zone where greater drag is induced. Very little tangible difference is observed between the water-TiO$_2$ (Fig. 3a) and ethylene glycol-TiO$_2$ nanofluids (Fig. 3b), despite the difference in viscosity of the base fluids.

Figs. 4a, b present the evolution of velocity gradient with semi-vertex angle (divergent, $\alpha < 0$) and Reynolds number (*Re*) with fixed momentum and thermal slip and weak viscous heating at nanoparticle volume fraction of 0.2. An increase in divergent semi-angle generally *retards* the flow from the centre line for the majority of the space until the near-wall zone where it induces a *weak acceleration*. The response is therefore opposite to that of increasing convergent angle (Figs. 3a,b). With greater divergence of the vertex, momentum distribution is adversely affected. The flow acceleration achieved with narrower angles is lost and the nanofluid flow behaves more like a diffuser system. This configuration is therefore better for more controlled deployment of fluids in medical devices e.g. nasal sprays [47], where more homogenous distribution of nanoparticles may be achieved in the core flow region. However convergent angles (Figs. 3a,b) are more suited to targeted, fast execution of drugs e.g. surface skin treatment (semi-powder-jet systems), divergent sections of de Laval nozzles in diabetic pumps [48] etc. Both geometric scenarios may therefore be exploited in different clinical applications. Figs. 4a and b, further demonstrate the principally decelerating influence of increasing Reynolds numbers. With greater inertial force (relative to viscous force), significant reduction in the flow is achieved for divergent channels, again testifying to the destruction of momentum in this type of geometry. These effects are computed for both water-TiO$_2$ (Fig. 4a) and ethylene glycol-TiO$_2$ nanofluids (fig. 4b), although slightly greater magnitudes of radial velocity gradient are attained in the former, in particular near and at the channel wall.

Figs. 5a, b illustrate the temperature distributions for various nano-particle volume fraction (ϕ) and thermal slip parameters (*b*) with fixed momentum slip and strong viscous heating at

Reynolds number of 40 and for a convergent channel. A substantial increase in temperature accompanies greater thermal slip values, for both water-TiO_2 (Fig. 5a) and ethylene glycol-TiO_2 nanofluids (fig. 5b). Thermal diffusion is therefore assisted with greater thermal jump at the channel wall. The nanofluid is significantly heated, although temperature is observed to drop from the centreline to the wall for any scenario. With greater nanoparticle volume fraction there is however a slight decrease in temperatures for water-TiO_2 (Fig. 5a) whereas there is more prominent reduction in temperature for ethylene glycol-TiO_2 nanofluid (fig. 5b). The general thermal enhancement properties of nanofluids, as predicted by many researchers, e.g. [24-26, 32], is therefore *not* computed for convergent channels.

Figs. 6a, b illustrate the temperature distributions for various semi-vertex angle (convergent, $\alpha > 0$) and Reynolds number (Re) with fixed momentum and thermal slip ($a = b = 0.5$), viscous heating ($Ec = 5$) and volume fraction ($\phi = 0.2$). Significantly higher temperatures are achieved with ethylene glycol-TiO_2 nanofluid (fig. 6b), than with water-TiO_2 (Fig. 6a) nanofluid. With greater semi-vertex angle, temperatures are strongly enhanced for both nanofluids. A wider channel convergent vertex therefore heats the nanofluid considerably compared with a narrower one. With greater Reynolds number, again a marked elevation in temperatures as achieved. A similar trend was reported also by Moradi *et al*. [35]

Figs. 7a,b present the influence of various semi-vertex angle (divergent, $\alpha < 0$) and Reynolds number (Re) again with fixed momentum and thermal slip ($a = b = 0.5$), viscous heating ($Ec = 5$) and volume fraction ($\phi = 0.2$). Converse to convergent channels, a substantial decrease in temperatures is caused with greater Reynolds numbers. However an increase in temperature does correspond to increasing divergent semi-vertex angle. Therefore both nanofluids are heated throughout the channel space irrespective of whether the vertex is converging or diverging. As with converging channels, however, greater temperatures are attained with ethylene glycol-TiO_2 nanofluid (fig. 7b) than with water-TiO_2 (Fig. 7a) nanofluid.

Figs 8a,b depict the skin friction plots for various thermophysical parameters. With greater nano-particle volume fraction (ϕ) a marked boost is achieved in skin friction, for both nanofluids, indicating considerable flow acceleration. Conversely with a small increase in Reynolds number, the flow is decelerated. This concurs with the trend in Fig. 3a where velocity gradients were noted to be lowered at the channel wall with greater Reynolds numbers. Approximately the same response is observed for both nanofluids i.e. the base fluid exerts very

little effect on the flow performance – the primary influence is from the nanoparticles, which as they are both Titanium oxide in figs 8a,b, do not alter profiles significantly. However the concentration of nano-particles simulated via the volume fraction clearly does modify the flow at the wall. Increasing momentum slip is also found to reduce skin friction.

Figs. 9a, b present the effects of velocity slip (a) and converging or diverging channel angles (α) for (a) Water-TiO_2 and (b) EG-TiO_2 nanofluids, on skin friction (C_f). With increasing momentum (velocity) slip skin friction is markedly depressed for both nanofluids. With increasing converging angle, skin friction is also decreased for both nanofluids, whereas with increasing diverging angle it is strongly increased.

Figs 10a, b illustrate Nusselt number (wall heat transfer rate) for various nano-particle volume fraction (ϕ), velocity slip (a) and Reynolds numbers (Re), again for a converging channel. Significant decay in Nusselt numbers accompanies increasing momentum slip values for both nanofluids. Generally Nusselt number is also enhanced with increasing Reynolds number and the effect is more pronounced as velocity slip increases. A strong elevation in Nusselt number is also observed with higher nanoparticle volume fraction. Higher concentrations of nano-particles therefore increase the transfer of heat from the nanofluid to the channel wall causing a drop in nanofluid temperature in the channel i.e. a cooling effect is induced. Distinct from the skin friction plots (Figs 9a,b), massively greater magnitudes of Nusselt number are achieved with EG-TiO_2 nanofluids (Fig 10b) compared with Water-TiO_2 nanofluids (Fig 10a) confirming that the base fluid has a prominent role in thermal enhancement of the nanofluid.

Figs 11a,b illustrate the influence of Eckert number (Ec), velocity slip (a) and converging-diverging channel angles (α) for (a) Water-TiO_2 and (b) EG-TiO_2 nanofluids. Again we note the enormously higher magnitudes of Nusselt number computed for EG-TiO_2 nanofluid in comparison with Water-TiO_2 nanofluid. With greater Eckert number, Nusselt number clearly demonstrates a *linear descent for diverging channels*, whereas it follows a *linear ascent for converging channels*. Heat transfer rate to the wall from the fluid is therefore greater for converging channels with higher Eckert number. This parameter which arises only in the heat conservation equation (13) embodies the relative significance of kinetic energy in the flow to enthalpy difference, as elaborated by Schlichting [1]. *Ec* >0 implies conversion of mechanical energy which is dissipated as heat in the nanofluid. This will heat the fluid and lead to greater

heat transfer from the fluid to the channel wall, as observed in the red solid lines in both Figs 11a,b. With increasing converging angle the rate of ascent of the Nusselt number profiles is increased, whereas with increasing diverging angle it is decreased. Heat transfer rate from the nanofluid to the wall therefore is boosted with wider convergent channels whereas it is depressed with wide divergent channels. The opposite effect will be induced in diverging channels, as testified to by the dotted green lines in both figs 11a, b.

7. CONCLUSIONS

A new transport model has been presented for *thermal and momentum slip effects on dissipative* nanofluid heat transfer and flow in a diverging/converging 2-D channel with solid walls. The Tiwari-Das nanofluid formulation has been implemented. The transformed boundary value problem is solved by **MAPLE 17**. Extensive validation has been achieved with the finite difference implicit Keller Box Method (**KBM**). The influence of nanoparticle volume fraction, Reynolds number, Prandtl number, channel semi-apex angle and Eckert (viscous dissipation) number are addressed. Properties of different nanofluids i.e. density ratio, thermal conductivity ratio and specific heat capacity ratio are evaluated using Tiwari-Das data for different nanoparticles (Titanium oxide, copper, alumina). Two nanofluids are considered- Water-TiO_2 and (b) Ethylene Glycol (EG)-TiO_2 nanofluid. The present computations have shown that with increasing velocity slip, for both water-TiO_2 and ethylene glycol-TiO_2 nanofluids, the channel bulk flow is decelerated. Similarly with greater solid (nanoparticle) volume and in the presence of momentum slip, the flow is also retarded. With increasing semi-vertex angle, the channel flow is generally accelerated although at the wall, the contrary behaviour is computed. An increase in divergent semi-angle on the other hand is found to generally decelerate the flow from the centre line for the core flow region, whereas near and at the channel wall it results in a *weak acceleration*. Higher temperatures are achieved with greater thermal slip values, for both water-TiO_2 and ethylene glycol-TiO_2 nanofluids, whereas for greater nanoparticle volume fraction, temperatures are weakly decreased for water-TiO_2 (Fig. 5a) whereas a more significant decreases is observed for ethylene glycol-TiO_2 nanofluid. With greater diverging channel angle, a substantial decrease in temperatures is caused with greater Reynolds numbers, and the reverse effect is computed for converging channels. The present model has neglected *non-Newtonian* properties [49] of the nanofluid and also *transient* effects [50, 51]- these will constitute future studies.

REFERENCES

[1] R.W. Niven, R.M. Kacmarek, J.D. Brain and R.A. Peterfreund, Small bore nozzle extensions to improve the delivery efficiency of drugs from metered dose inhalers: laboratory evaluation, *Amer. Rev. Respir. Dis*., 147, 1590-4 (1993).

[2] T. Ozeki and T. Tagami, Drug/polymer nanoparticles prepared using unique spray nozzles and recent progress of inhaled formulation, *Asian J. Pharmaceutical Sciences*, 9, 236–243 (2014).

[3] T. Ozeki, Y. Akiyama, N. Takahashi, *et al.,* Development of a novel and customizable two-solution mixing type spray nozzle for one-step preparation of nanoparticle-containing microparticles, *Biol. Pharm. Bull.*, 35, 1926–1931 (2012).

[4] X-D. Wang, Y.-X. Huang, C-H. Cheng, J.-Y. Jang and D. J. Lee, An inverse geometry design problem for optimization of single serpentine flow field of PEM fuel cell, *Int. J. Hydrogen Energy*, 35, 4247 – 4257 (2010).

[5] H. Schlichting, *Boundary-Layer Theory*, MacGrawHill, New York, 8th edn (2000).

[6] R.T. Balmer and J.J. Kauzlaich, Similarity solutions for the converging or diverging steady flow of non-Newtonian elastic power law fluids with wall suction or injection-Part I: Two-dimensional channel flow, *AIChem. J*., 17, 1181–1188 (1971).

[7] A. Hooper, B. R. Duffy, H. K. Moffatt, Flow of fluid of non-uniform viscosity in converging and diverging channels,*J . Fluid Mech.,* **117,** 283 – 304 (1982).

[8] P. Hariharan, V. Seshadri, R. K. Banerjee, Peristaltic transport of non-Newtonian fluid in a diverging tube with different wave forms, *Mathematical and Computer Modelling*, 48, 998–1017 (2008).

[9] C-Y. Wu and R.-T. Tsai, Fluid mixing via multidirectional vortices in converging–diverging meandering microchannels with semi-elliptical side walls, *Chemical Engineering J.*, 41, 320–328 (2013).

[10] J. Lamont, S. Ramesh, S. V. Ekkad, A. Tolpadi, C. Kaminski and S. Salah, Heat transfer enhancement in narrow diverging channels, *ASME J. Turbomachinery*, 135(4), 04101(2013).

[11] E. Stalio and M. Piller, Direct numerical simulation of heat transfer in converging–diverging wavy channels, *ASME* [12] S. Nadeem, N. S. Akbar, N. Bibi, and S. Ashiq, Influence of heat and mass transfer on peristaltic flow of a third order fluid in a diverging tube, *Comm. Nonlinear Science and Numerical Simulation*, 15, 2916–2931 (2010).

[12] S. Choi, Enhancing thermal conductivity of fluids with nanoparticles, *Developments and applications of non-Newtonian flows, D. A. Siginer and H. P., Wang, eds., American Society of Mechanical Engineers, New York, FED-* Vol. 231/MD- 66, 99–105 (1995).

[13] L. Hendraningrat, S. Li and O. Torsæter, A coreflood investigation of nanofluid enhanced oil recovery, *Petroleum Science and Engineering*, 111, 128–138 (2013).

[14] A. Ebaid and H. Emad Aly, Exact analytical solution of the peristaltic nanofluids flow in an asymmetric channel with flexible walls and slip condition: application to cancer treatment, *Computational and Mathematical Methods in Medicine*, vol. 2013, Article ID 825376, 8 pages (2013).

[15] V.R. Prasad, S. A. Gaffar and O. Anwar Bég, Non-similar computational solutions for free convection boundary-layer flow of a nanofluid from an isothermal sphere in a non-Darcy porous medium, *J. Nanofluids*, 4, 1–11 (2015).

[16] Tombácz E., Bica D., Hajdú A., Illés E., Majzik A., Vékás L., Surfactant double layer stabilized magnetic nanofluids for biomedical application, *J. Phys Condens Matter*., 20, 204103 (2008).

[17] M.J. Uddin, O. Anwar Bég and N.S. Amin, Hydromagnetic transport phenomena from a stretching or shrinking nonlinear nanomaterial sheet with Navier slip and convective heating: a model for bio-nano-materials processing, *J. Magnetism Magnetic Materials,* 368, 252-261(2014).

[18] O. Anwar Bég, M. Ferdows, Shamima Islam and M. Nazrul Islam, Numerical simulation of Marangoni magnetohydrodynamic bio-nanofluid convection from a non-isothermal surface with magnetic induction effects: a bio-nanomaterial manufacturing transport model, *J. Mechanics Medicine Biology*, 14, 1450039.1-1450039.32 (2014).

[19] O. Anwar Bég, V.R. Prasad, B. Vasu, Numerical study of mixed bioconvection in porous media saturated with nanofluid and containing oxytactic micro-organisms, *J. Mechanics Medicine Biology,* 13, 1350067 .1-1350067.25 (2013).

[20] W.H. De Jong and P. Borm. Drug delivery and nanoparticles: Applications and hazards, *Int. J. Nanomedicine,* 3, 133–149 (2008).

[21] J.M. Nam, C.C. Thaxton, and C.A. Mirkin, Nanoparticles-based bio-bar codes for the ultrasensitive detection of proteins, *Science,* 301, 1884–1886 (2003).

[22] S. Das, S.U.S. Choi, W. Yu, T. Pradeep, *Nanofluids: Science and Technology*, 1^{s}t ed., Wiley, New York (2007).

[23] Y. Xuan, Q., Li, Investigation on convective heat transfer and flow features of nanofluids, *ASME J. Heat Transfer* 125(1) (2003) 151–155.

[24] D. Wen, Y. Ding, Natural convective heat transfer of suspensions of titanium dioxide nanoparticles (Nanofluids), *IEEE Trans. Nanotechnol*. 5(3) (2006) 220–227.

[25] H. Adnan, M.K.V. Sharma, R.A. Bakar, K. Kadirgama, A review of forced convection heat transfer enhancement and hydrodynamic characteristics of a nanofluid, *Renewable and Sustainable Energy Reviews*, 29 (2014)734-743.

[26] R.K. Tiwari, M.K. Das, Heat transfer augmentation in a two-sided lid-driven differentially heated square cavity utilizing nanofluids, *Int. J. Heat Mass Transf*. 50 (2007) 2002–2018.

[27] D. Tripathi, and O. Anwar Bég, A study on peristaltic flow of nanofluids: application in drug delivery systems, *Int. J. Heat Mass Transfer* 70 (2014) 61–70.

[28] Akbar NS, Nadeem S, Peristaltic flow of a Phan-Thien-Tanner nanofluid in a diverging tube, *Heat Transf Res.*, 41 (2012) 10–22.

[29] Dinarvand S. Nodal/saddle stagnation-point boundary layer flow of CuO–Ag/water hybrid nanofluid: a novel hybridity model. Microsystem Technologies. 2019 Jul;25(7):2609-23.

[30] Mousavi, S. M., Rostami, M. N., Yousefi, M., Dinarvand, S., Pop, I., & Sheremet, M. A. (2021). Dual solutions for Casson hybrid nanofluid flow due to a stretching/shrinking sheet: A new combination of theoretical and experimental models. *Chinese Journal of Physics*, *71*, 574-588.

[31] Dinarvand, S., & Rostami, M. N. (2020). Three-dimensional squeezed flow of aqueous magnetite–graphene oxide hybrid nanofluid: A novel hybridity model with analysis of shape factor effects. *Proceedings of the Institution of Mechanical Engineers, Part E: Journal of Process Mechanical Engineering*, *234*(2), 193-205.

[32] Dinarvand, S., Mousavi, S. M., Yousefi, M., & Rostami, M. N. (2021). MHD flow of MgO-Ag/water hybrid nanofluid past a moving slim needle considering dual solutions: an applicable model for hot-wire anemometer analysis. *International Journal of Numerical Methods for Heat & Fluid Flow*

[33] R. E. White and V. R. Subramanian, *Computational Methods in Chemical Engineering with Maple*, Springer, New York, NY, USA (2010).

[34] O. Anwar Bég, M.M. Rashidi, M. Akbari, A. Hosseini, Comparative numerical study of single-phase and two-phase models for bio-nanofluid transport phenomena, *J. Mechanics in Medicine and Biology* (2013). DOI: 10.1142/S0219519414500110 (35 pages)

[35] A Moradi, A. A Alsaedi, A. A Hayat, Investigation of nanoparticles effect on the Jeffery–Hamel Flow, *Arabian J. Science and Engineering*, 38, 2845-2853 (2013).

[36] Md. Jashim Uddin, O. Anwar Bég and Ahmad Izani Md. Ismail, Mathematical modelling of radiative hydromagnetic thermo-solutal nanofluid convection slip flow in saturated porous media, *Math. Prob. Engineering,* 2014, Article ID 179172, 11 pages (2014).

[37] Beg, O. Anwar, M. J. Uddin, T. Bég, and R. Reddy Gorla. Numerical simulation of self-similar thermal convection from a spinning cone in anisotropic porous medium. Journal of Hydrodynamics, Ser. B 28, no. 2 (2016): 184-194.

[38] Md. Jashim Uddin, N.H. Md. Yusoff, O. Anwar Beg and Ahamd Izani Ismail, Lie group analysis and numerical solutions for non-Newtonian nanofluid flow in a porous medium with internal *heat generation, Physica Scripta,* **87***,* 025401 (14pp) (2013).

[39] J. Zueco and O. Anwar Bég, Network numerical simulation of hydromagnetic Marangoni mixed convection boundary layers, *Chemical Engineering Communications,* 198, 4, 552-571 (2010).

[40] O. Anwar Bég and O.D. Makinde, Viscoelastic flow and species transfer in a Darcian high-permeability channel, *Petroleum Science and Engineering,* **76**, 93–99 (2011).

[41] V. R. Prasad, S. A. Gaffar and O. Anwar Bég, Heat and mass transfer of a nanofluid from a horizontal cylinder to a micropolar fluid, *AIAA J. Thermophysics Heat Transfer,* 29, 1, 127-139 (2015).

[42] S. Abdul Gaffar, V. Ramachandra Prasad and O. Anwar Bég, Computational analysis of magnetohydrodynamic free convection flow and heat transfer of non-Newtonian tangent hyperbolic fluid from a horizontal circular cylinder with partial slip, *Int. J. Appl. Comput. Math*. (2015). **DOI 10.1007/s40819-015-0042-x** (25pages)

[43] O. Anwar Bég, M. J. Uddin and W.A. Khan, Bioconvective non-Newtonian nanofluid transport in porous media containing micro-organisms in a moving free stream, *J. Mechanics Medicine Biology,* 15, 1550071.1-1550071.20 (2015).

[44] H. B. Keller, Numerical methods in boundary-layer theory, *Ann. Rev. Fluid Mechanics*, 10, 417–433 (1978).

[45] A. Moradi, A. Alsaedi and T. Hayat, investigation of heat transfer and viscous dissipation effects on the Jeffery-Hamel flow of nanofluids, *Thermal Science*, 19, 563-578 (2015).

[46] Minkowycz, W., *et al*. (Ed), *Nanoparticle Heat Transfer and Fluid Flow*, CRC Press, Taylor & Francis, USA (2013).

[47] K. Inthavong, J. Tu, Numerical modelling of nanoparticle deposition in the nasal cavity and the tracheobronchial airway, *Computer Methods in Biomechanics and Biomedical Engineering*, 14, 633-43 (2011).

[48] C.Y. Li *and 13 others*, Needle-free injection of insulin powder: delivery efficiency and skin irritation assessment *J Zhejiang Univ-Sci B (Biomed & Biotechnol),* 14, 888-899 (2014).

[49] S. Abdul Gaffar, V. R. Prasad and O. Anwar Bég, Numerical study of flow and heat transfer of non-Newtonian tangent hyperbolic fluid from a sphere with Biot number effects, *Alexandria Engineering J.* (2015). DOI.ORG/10.1016/J.AEJ.2015.07.001. (13 pages)

[50] V. Rajesh, M.P. Mallesh and O. Anwar Bég, Transient MHD free convection flow and heat transfer of nanofluid past an impulsively started vertical porous plate in the presence of viscous dissipation, *Procedia Materials Science,* 10, 80-89 (2015).

[51] A. Zaman, N. Ali and O. Anwar Bég, Unsteady magnetohydrodynamic blood flow in a porous-saturated overlapping stenotic artery: Numerical modelling, *J. Mechanics in Medicine and Biology* (2015). DOI: 10.1142/S0219519416500494 (16 pages)